

Waveguide Microwave Imaging: Neural Network Reconstruction of Functional 2-D Permittivity Profiles

Alexander V. Brovko, *Member, IEEE*, Ethan K. Murphy, and Vadim V. Yakovlev, *Senior Member, IEEE*

Abstract—A new microwave imaging technique is proposed for reconstruction of 2-D complex permittivity profiles in dielectric samples located in a waveguide system. The spatial distributions of the dielectric constant and the loss factor are approximated by continuous functions whose functional parameters are determined using a neural network technique backed by full-wave finite-difference time-domain analysis. The profiles are reconstructed from measurements of reflection and transmission characteristics obtained with the tested sample at different locations. Operational capabilities of the technique are illustrated through a series of computational experiments for rectangular and cylindrical samples at two (original and 90°-rotated) positions. The results demonstrate excellent agreement between the reconstructed and actual profiles approximated by linear, quadratic, and Gaussian functions: the average relative errors do not exceed 0.4%, 2.2%, and 4.8%, respectively. Finally, the assumption of functional approximation, uniqueness of the reconstruction, and prospects of practical use of the technique are thoroughly discussed.

Index Terms—Artificial neural network (ANN), finite-difference time-domain (FDTD) simulation, microwave imaging, model functions, permittivity profile, S -parameters, waveguide.

I. INTRODUCTION

MICROWAVE imaging of spatial distribution of complex permittivity inside dielectric objects is an important technology of nondestructive evaluation (NDE) and testing [1] due to its potential functional benefits for many applications, such as medical diagnostics (detection of inhomogeneities in distribution of tissues) [2], [3], recognition of defects and cracks in construction materials [4], composite panels [5], wood slabs [6], and many others.

Our interest in this technology is conditioned by the principal obstacle in the development of controllable microwave sintering of particulate and powder materials—the lack of knowledge about behavior of dielectric and thermal properties of the

samples in the course of their sintering [7], [8]. The absence of reliable data of material parameters effectively slows down the progress in modeling of microwave heating of metal powder: the known studies are limited to fairly idealistic computational schemes (e.g., [9]) and much of the work in microwave sintering thus far is still restricted to experimental studies [8]. Since there are substantial difficulties in measuring media parameters nonuniformly distributed inside the material at temperatures of hundreds degrees Celsius, contactless microwave imaging may be an attractive approach in getting spatial profiles of effective permittivity of the sintered objects.

Numerical solutions of inverse problems are widely considered a crucial part of the applied technologies of NDE, and a technique capable of reconstructing spatial profiles of complex permittivity ($\varepsilon = \varepsilon' - i\varepsilon''$) appears to be one of the most needed tools required for adequate modeling of microwave sintering. However, the existing 1-D approaches (e.g., [10]–[13]) do not seem practical here, and the reported techniques of reconstruction of 2-D and 3-D permittivity profiles (e.g., [2]–[4] and [14]–[16]) are associated with complex experimental implementations, characterized by relatively low resolution and accuracy, and developed for open scenarios. While it has been shown that artificial neural network (ANN)-based techniques may be efficient in the determination of complex permittivity of homogeneous materials [17]–[19], the known ANN methods of reconstruction of nonuniform distribution of the dielectric constant ε' and the loss factor ε'' are applicable only to the coaxial [20] or layered [21] structures and deal effectively with 1-D reconstruction. On the other hand, recently, an ANN method has been successfully used for detecting a 3-D position and size of a spherical inclusion in a dielectric sample located in a waveguide system [22].

In this paper, we describe a new ANN technique, which reconstructs 2-D complex permittivity profiles from elementary measurements in a closed system. The technique deals with S -parameters of a waveguide containing the tested sample. The profiles $\varepsilon'(x, y)$ and $\varepsilon''(x, y)$ are described by continuous functions defined by a small number of coefficients (in this study, we consider linear, quadratic, and Gaussian functions), and an ANN is used for reconstruction of functional parameters controlling the profile. The network is trained by numerical data generated by multiple full-wave 3-D finite-difference time-domain (FDTD) analysis of the entire waveguide system with the sample at different locations; functionality of the method is shown for the objects in their original and rotated positions. We, therefore, provide here a detailed account of

Manuscript received August 04, 2008; revised October 20, 2008. First published January 19, 2009; current version published February 06, 2009. This work was supported in part by the EADS Company Foundation, the German Academic Exchange Service (DAAD), and the Ministry of Education and Science of the Russian Federation.

A. V. Brovko is with the Department of Applied Information Technologies, Saratov State Technical University, Saratov 410070, Russia (e-mail: brovkoav@gmail.com).

E. K. Murphy and V. V. Yakovlev are with the Department of Mathematical Sciences, Worcester Polytechnic Institute, Worcester, MA 01609 USA (e-mail: ekmurphy@wpi.edu; vadim@wpi.edu).

Color versions of one or more of the figures in this paper are available online at <http://ieeexplore.ieee.org>.

Digital Object Identifier 10.1109/TMTT.2008.2011203

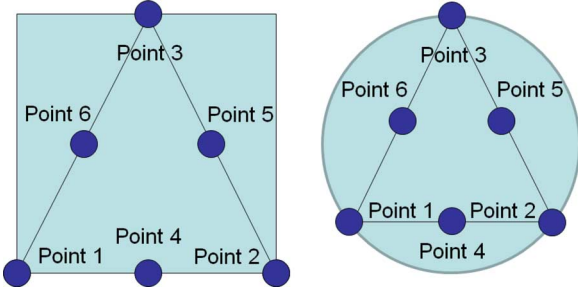


Fig. 1. Locations of the base points in reconstruction of linear and quadratic polynomial functions in 2-D rectangular and cylindrical samples.

the technique being more general, more advanced, and more accurate in comparison with the procedure that was earlier summarized and tested for a Gaussian model function in [23].

Since, to the best of our knowledge, no general techniques of microwave imaging in closed systems have been developed thus far, this paper aims to suggest a first stage of an original approach to their design. Here we start with the assumption of a known functional approximation of a 2-D profile and focus on a variety of essential technical issues: concept of an ANN solution (S -parameters as the network input and functional parameters as the network output), operational characteristics of the neural network technique, its functionality when working with different functions, amount and type of data sufficient for reconstruction of profiles, etc. These issues may be considered a conceptual background for the subsequent development of ANN-based reconstructors of arbitrary 2-D, functional 3-D, and arbitrary 3-D profiles.

II. METHOD

Our approach to finding 2-D complex permittivity profiles is built on the idea of approximation of spatial distributions $\varepsilon'(x, y)$ and $\varepsilon''(x, y)$ by some surfaces described by smooth continuous functions that are defined by a small number of independent coefficients. The reconstruction is then reduced to the determination of either a set of functional coefficients or a set of values of ε' and ε'' at some points in the domain such that most close correspondence between the actual distribution and the model function would be provided.

Flexibility of our approach in reconstructing a variety of the profiles is maintained by the model function taking different configurations depending on its coefficients. In this paper, we explore the potential of the technique dealing with three types of the model function, namely, linear, quadratic, and Gaussian, approximating the actual surfaces $\varepsilon'(x, y)$ and $\varepsilon''(x, y)$.

In order to find six unknown coefficients c'_1, \dots, c'_3 in the linear functions

$$\begin{aligned}\varepsilon'(x, y) &= c'_1 + c'_2x + c'_3y \\ \varepsilon''(x, y) &= c''_1 + c''_2x + c''_3y\end{aligned}\quad (1)$$

six values of the functions $\varepsilon'(x, y)$ and $\varepsilon''(x, y)$ are required, so we take them from three base points located in the sample. The locations of these points are arbitrary if they do not lie on a line, thus we choose them as Points 1–3 in Fig. 1.

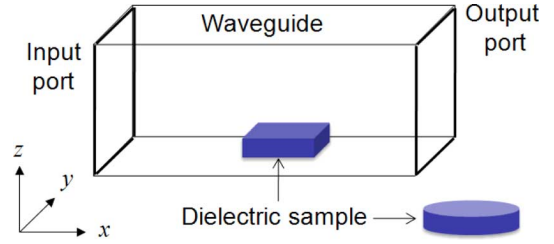


Fig. 2. Measurement system with a rectangular/cylindrical 2-D sample.

For quadratic polynomials

$$\begin{aligned}\varepsilon'(x, y) &= c'_1 + c'_2x + c'_3y + c'_4xy + c'_5x^2 + c'_6y^2 \\ \varepsilon''(x, y) &= c''_1 + c''_2x + c''_3y + c''_4xy + c''_5x^2 + c''_6y^2\end{aligned}\quad (2)$$

we need the functional values $\varepsilon'(x_1, y_1), \dots, \varepsilon''(x_6, y_6)$ in six base points to find 12 unknown coefficients; these points are chosen as Points 1–6 (Fig. 1). Our choice of positions of the points is suggested by the behavior of the function defined by a simplex element in the finite-element method.

When dealing with linear and quadratic functions, our technique determines the functional value in the base points, whereas in the case of Gaussian approximations in the form of

$$\begin{aligned}\varepsilon'(x, y) &= a' \left[1 + b' \exp \left(-\frac{(x-x'_0)^2 + (y-y'_0)^2}{r_0'^2} \right) \right] \\ \varepsilon''(x, y) &= a'' \left[1 + b'' \exp \left(-\frac{(x-x''_0)^2 + (y-y''_0)^2}{r_0''^2} \right) \right]\end{aligned}\quad (3)$$

we reconstruct independent coefficients. In (3), x_0 and y_0 are the parameters responsible for the position of the maximum (or minimum) of the function, r_0 controls the width of the peak at the level of $\exp(-1)$ from the maximum, and b and a define the functional values at the extreme point and at infinity from the peak, respectively. Due to these controlling mechanisms provided by the coefficients, the Gaussian surface may be suitably “bendable” in describing fairly different spatial distributions of the dielectric constant and the loss factor.

Furthermore, we combine the idea of functional approximation of the permittivity profiles with the numerical model representing an experimental system chosen as a simple waveguide structure proven to be convenient in ANN-based reconstruction of complex permittivity of uniform samples [18], [19]. The measurement system consists of a rectangular waveguide with two (input and output) ports containing a dielectric sample lying on the narrow waveguide’s wall (Fig. 2). The measured parameters are complex reflection (S_{11}) and transmission (S_{21}) coefficients.

The ANN used for reconstruction of the permittivity profiles and shown in Fig. 3 is a radial basis function (RBF) network with cubic basis function [24]. The ANN inputs are the values of $(4 \times P)$ S -parameters obtained for P positions of the sample. The ANN outputs are the model function’s parameters defining spatial distribution of complex permittivity; in this paper, they

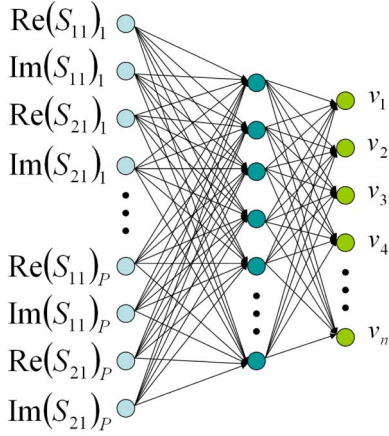


Fig. 3. Architecture of the ANN for reconstruction of functional coefficients.

are considered, depending on the type of the function, as the vectors

$$\begin{bmatrix} v_1 \\ \vdots \\ v_n \end{bmatrix} = \begin{cases} [\varepsilon'(x_1, y_1) \dots \varepsilon'(x_3, y_3) \varepsilon''(x_1, y_1) \dots \varepsilon''(x_3, y_3)]^T, & \text{for (1)} \\ [\varepsilon'(x_1, y_1) \dots \varepsilon'(x_6, y_6) \varepsilon''(x_1, y_1) \dots \varepsilon''(x_6, y_6)]^T, & \text{for (2)} \\ [a'b'x_0'y_0'r_0'a''b''x_0''y_0''r_0'']^T, & \text{for (3)}. \end{cases} \quad (4)$$

In this formulation, the resolution of reconstruction of a permittivity profile is independent of the ANN structure and, in particular, of the number of outputs that may be impractically large if each output is associated directly with the material parameters of a particular point/portion of the tested sample. In that case, the control over the resolution of reconstruction can be maintained by working with characteristics of our predefined functions. On the other hand, with the form (4), the ANN technique has more flexibility and the potential for quicker operations with relatively simple profiles in comparison with the architecture in [23] structured for independent coefficients only.

We can represent the inputs and the outputs as the matrices

$$\mathbf{X} = \begin{bmatrix} \text{Re}(|S_{11}|)_1^1 & \text{Im}(|S_{11}|)_1^1 & \cdots & \text{Im}(|S_{21}|)_1^P \\ \vdots & \vdots & \ddots & \vdots \\ \text{Re}(|S_{11}|)_D^1 & \text{Im}(|S_{11}|)_D^1 & \cdots & \text{Im}(|S_{21}|)_D^P \end{bmatrix} \quad (5)$$

$$\mathbf{Y} = \begin{bmatrix} v_{11} & v_{12} & \cdots & v_{1n} \\ v_{21} & v_{22} & \cdots & v_{2n} \\ \vdots & \vdots & \ddots & \vdots \\ v_{D1} & v_{D1} & \cdots & v_{Dn} \end{bmatrix} \quad (6)$$

respectively. In (5) and (6), D is the number of samples of input–output pairs. The RBF network is coupled with a linear model

$$\tilde{\mathbf{Y}} = \mathbf{X}\mathbf{W}_1 + \tilde{\Phi}(\mathbf{X})\mathbf{W}_2 = \Phi(\mathbf{X})\mathbf{W} \quad (7)$$

where $\mathbf{W} = [\mathbf{W}_1 \mathbf{W}_2]$ is the weight matrix and the matrix Φ can be described component-wise as

$$\Phi_{ij} = \begin{cases} X_{ij}, & \text{if } j \leq n \\ 1, & \text{if } j = n + 1 \\ \|X_i - C_{j-n-1}\|_2^2, & \text{otherwise.} \end{cases} \quad (8)$$

The first two components of (8) represent the linear problem and the last component is the RBF network.

In order to train the network, we partition the input–output pairs in training and testing sets $\mathbf{S}_1 = \{\mathbf{X}^{(1)}, \mathbf{Y}^{(1)}\}$ and $\mathbf{S}_2 = \{\mathbf{X}^{(2)}, \mathbf{Y}^{(2)}\}$ and, similar to [24], use a zero training error technique [25] that assumes that the set of centers, \mathbf{C} , is the same as $\mathbf{X}^{(1)}$.

The weights of the network are found with a least squares approach—we attempt to minimize the error

$$\mathbf{E}(\mathbf{W}) = \frac{1}{2} \|\mathbf{Y}^{(1)} - \Phi(\mathbf{X}^{(1)})\mathbf{W}\|_2. \quad (9)$$

Differentiating (9) with respect to \mathbf{W} , we get the solution in the form

$$\mathbf{W} = (\Phi_1^T \Phi_1)^{-1} \Phi_1^T \mathbf{Y}^{(1)}. \quad (10)$$

where $\Phi_1 = \Phi(\mathbf{X}^{(1)})$. The matrix $\Phi_1^T \Phi_1$ is inverted using truncated singular value decomposition; this step, therefore, involves regularization. With the use of the weights from (10) and (7), we have our function that approximates the surface from $4 \times P$ given measurements.

It has been found that S -parameters of the structure in Fig. 2 are notably sensitive to nonuniformity of permittivity only in the direction of field propagation (the x -axis). This is consistent with the fact that the electric field of the TE₁₀ mode is constant along the y -axis, and thus, does not “respond” to the discontinuities in this direction. This suggests that in order to retrieve information about $\varepsilon'(x, y)$ and $\varepsilon''(x, y)$, one can deal with S -parameters corresponding to different samples’ positions in the xy -plane, e.g., such that the next position is taken as an α° rotation of the previous one. Thus, P sets of S -parameters associated with the ANN input correspond in our study to the original and rotated positions of the sample. Rotation of a tested sample has been found to be an efficient trick to increase the resolution of waveguide microwave imaging [22].

The elements of matrix (6), the network output, are picked up as random combinations of functional parameters uniformly distributed in the specified intervals. Corresponding S -parameters [i.e., the elements of matrix (5)] are obtained with the use of the full-wave 3-D conformal FDTD simulator QuickWave-3D [26]. The network is then trained with the input–output pairs (5) and (6).

Specifically, the ANN is trained with D points, and then we evaluate the network error from the testing data. D is increased until the error is sufficiently low—corresponding criterion, depending on the problem, may be conditioned by a maximum deviation in all network responses or by an average deviation. Once quality of learning characterized by the network error appears satisfactory, the ANN is deemed able to reconstruct

$[v_1 \dots v_n]^T$ (and thus, $\varepsilon'(x, y)$ and $\varepsilon''(x, y)$) using the $4 \times P$ S -parameters obtained from the related measurements.

The reconstruction algorithm is implemented as a MATLAB code.

III. RESULTS

In this section, we present the numerical results obtained for two shapes of the tested sample—a rectangular box and a cylinder (Fig. 2)—with no variation of complex permittivity along the z -axis.

Reconstructions are performed in the section of WR975 (248 mm \times 124 mm) of the length 612 mm operating at 915 MHz and containing the rectangular (60 mm \times 60 mm and height 20 mm) or cylindrical (diameter 60 mm and height 20 mm) samples. The values of the dielectric constant and the loss factor of the profiles are supposed to be within the intervals $1 \leq \varepsilon' \leq 10$ and $0 \leq \varepsilon'' \leq 6$ for functions (1) and (3) and $10 \leq \varepsilon' \leq 15$ and $10 \leq \varepsilon'' \leq 15$ for (2).

All results presented in this section (except the one illustrated by Table I) are obtained with the simplest scenario when the profiles given by linear, quadratic, and Gaussian functions are reconstructed with only two positions of the samples (i.e., for $P = 2$, or 8 ANN input parameters), namely, with $\alpha = 90^\circ$.

In the FDTD model, we employ a nonuniform mesh with 2 mm \times 2 mm \times 2 mm cells within the samples and 9 mm \times 9 mm \times 9 mm cells outside them. For both the rectangular and cylindrical samples, the total numbers of cells in the model is nearly 163 000 (16 MB of RAM). Steady state is supposed to be reached after 8000 time steps—for a Xeon 3.2-GHz PC operating under Windows XP, it takes 1.7 min of CPU time.

To evaluate the accuracy of reconstruction, a difference between the two surfaces is evaluated through an average relative error

$$\bar{E} = \frac{E}{\bar{F}_a} 100\% \quad (11)$$

where an average absolute error E and an average function value \bar{F}_a are defined as

$$E = \frac{1}{S} \int_S |F_a(x, y) - F_r(x, y)| dS \quad (12)$$

$$\bar{F}_a = \frac{1}{S} \int_S F_a(x, y) dS \quad (13)$$

F_a and F_r are the values of the actual and reconstructed functions at the point (x, y) , respectively, and S is the area of the sample in the xy -plane.

In the examples below, the quality of network learning is evaluated through the average deviation of the network responses \mathbf{v}_n from the actual values of the testing points \mathbf{v}_t

$$\hat{E} = \frac{\sum_{i=1}^{D_t} \|\mathbf{v}_t - \mathbf{v}_n\|_2}{\sum_{i=1}^{D_t} \|\mathbf{v}_t\|_2} 100\% \quad (14)$$

where D_t is the number of testing points. Vectors \mathbf{v}_t and \mathbf{v}_n in (14) are determined by the structure of the network output (4).

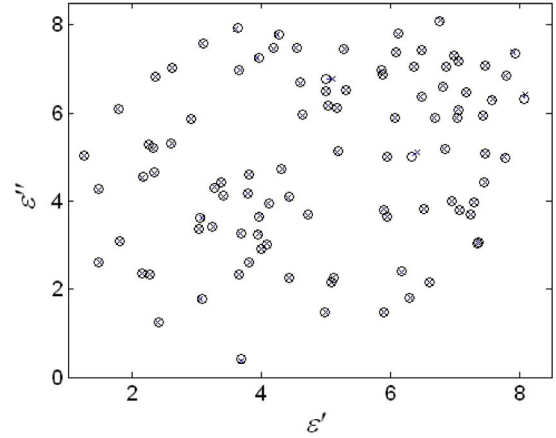


Fig. 4. Network responses (\times) to testing points (\circ) in reconstruction of complex permittivity values in base point 1; rectangular sample; linear model function; 400 training and 100 testing points; $\bar{E} = 0.3\%$.

A. Linear Function

The following results are obtained in reconstructions of permittivity profiles varying as linear functions (1). Fig. 4 illustrates excellent network learning in reconstruction of ε' and ε'' in one of the base points; for other points, the network responses are very similar, thus the respective patterns are not shown.

In Fig. 5, the test planes given as

$$\begin{aligned} \varepsilon'(x, y) &= 5 + 0.0667x - 0.0333y \\ \varepsilon''(x, y) &= 3 + 0.0100x + 0.0233y \end{aligned} \quad (15)$$

are shown along with the reconstructed ones. The planes are virtually indistinguishable; the average absolute/relative errors E/\bar{E} for $\varepsilon'(x, y)$ and $\varepsilon''(x, y)$ are 0.005/0.1% and 0.011/0.4%, respectively.

B. Quadratic Function

Here, the functionality of our technique is tested with the profiles given by quadratic functions (2). Typical performance of the algorithm in reconstructing ε' and ε'' is shown in Fig. 6 for one of the base points. The quality of network learning is seen to be not as good as shown in Fig. 4, but considering that here the network features six outputs and is trained by only slightly more training points than in the linear case (Section III-A), this may appear not too surprising.

The quadratic test surfaces set as

$$\begin{aligned} \varepsilon'(x, y) &= 9 + 0.0667x + 0.0044x^2 + 0.0056y^2 \\ \varepsilon''(x, y) &= 15.75 - 0.0667x + 0.0333y - 0.0033x^2 \\ &\quad - 0.0008y^2 \end{aligned} \quad (16)$$

are plotted in Fig. 7 along with the reconstructed profiles. The surfaces still seem to be very close to each other with the average absolute/relative errors 0.256/2.2% and 0.201/1.4% for $\varepsilon'(x, y)$ and $\varepsilon''(x, y)$, respectively.

C. Gaussian Function

In testing our technique with surfaces given by Gaussian functions, we simplify the problem by setting $x'_0 = x''_0 = x_0$, $y'_0 = y''_0 = y_0$, and $r'_0 = r''_0 = r_0$. By having these three

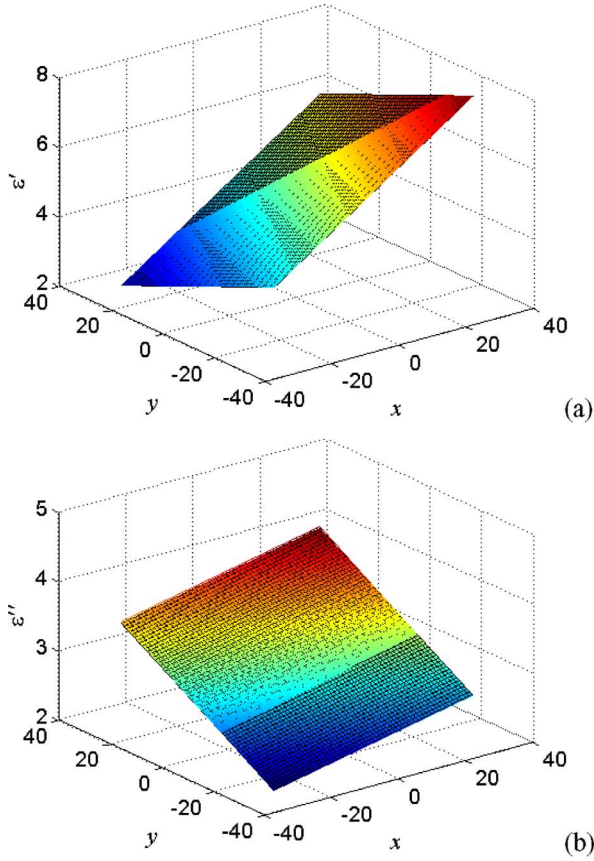


Fig. 5. Actual linear complex permittivity profiles given by (15) (transparent surfaces) and reconstructed profiles (solid surface): (a) $\varepsilon'(x, y)$ and (b) $\varepsilon''(x, y)$; rectangular sample.

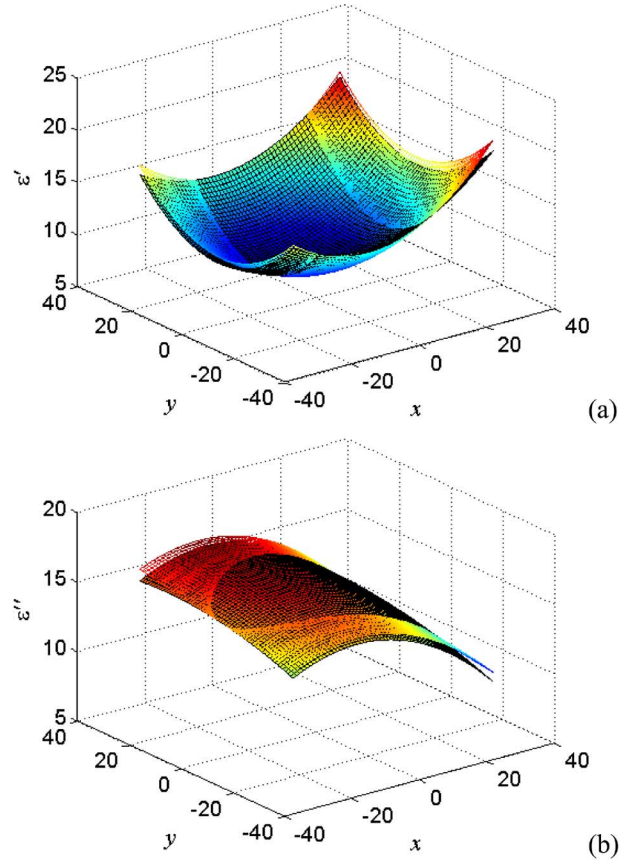


Fig. 7. Actual quadratic complex permittivity profiles given by (16) (transparent surfaces) and reconstructed profiles (solid surfaces): (a) $\varepsilon'(x, y)$ and (b) $\varepsilon''(x, y)$; rectangular sample.

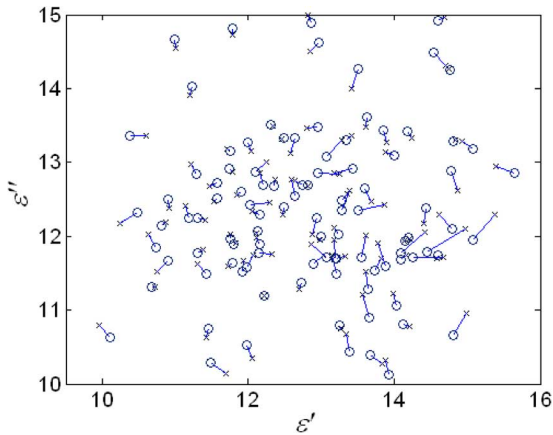


Fig. 6. Network responses (\times) to testing points (\circ) in reconstruction of complex permittivity values in base point 6; rectangular sample; quadratic model function; 476 training and 100 testing points; $\tilde{E} = 2.6\%$.

parameters be the same for both ε' and ε'' , we agree that the profiles of the dielectric constant and the loss factors are not fully independent. While this assumption makes the technique applicable to a narrower class of materials, the only goal for this simplification in the present example is to reduce the number of parameters responsible for spatial distribution of both characteristics to seven and decrease the computational cost of the problem.

First, we characterize the technique in its operation with Gaussian permittivity profiles by Fig. 8 showing the network performance in finding the coefficients a' , a'' , and the parameters $d' = a'(1 + b')$ and $d'' = a''(1 + b'')$, which are introduced for controlling behavior of Gaussian functions by two independent parameters in place of b' and b'' , which are dependent on a' and a'' . The network responses are seen to be a very good match to the actual values of the functional parameters.

We also characterize the accuracy of the technique in handling the Gaussian model function by the average total squared error \tilde{E} constructed as

$$\tilde{E} = \frac{1}{100} \sum_{i=1}^{100} \left\{ \left[a_a^{(i)} - a_r^{(i)} \right]^2 + \left[a_a''^{(i)} - a_r''^{(i)} \right]^2 + \left[d_a^{(i)} - d_r^{(i)} \right]^2 + \left[d_a''^{(i)} - d_r''^{(i)} \right]^2 \right\} \quad (17)$$

where the squared terms are summed for 100 randomly chosen test points and the indices a and r denote the actual and reconstructed parameters, respectively. Fig. 9 illustrates the convergence of our technique in reconstructing the indicated seven parameters in scenarios with rectangular and cylindrical samples—the curves show the behaviors of typical errors versus a

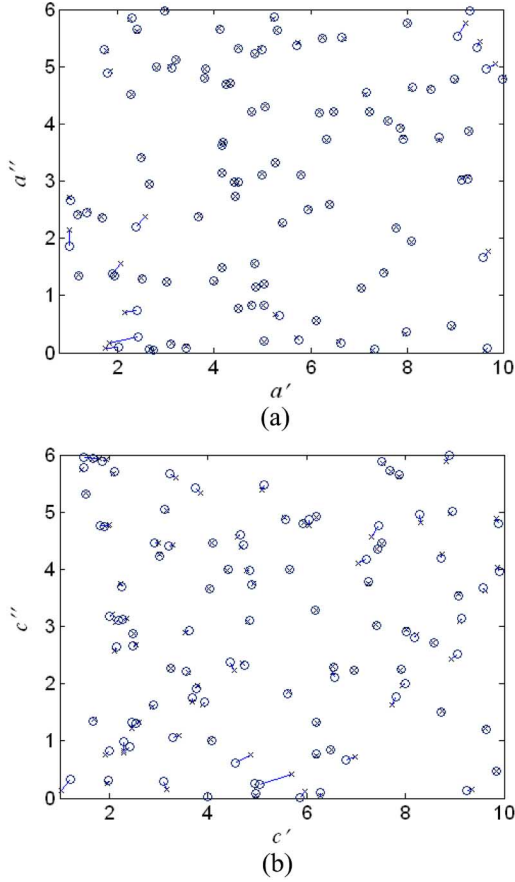


Fig. 8. Network responses (\times) to testing points (o) in reconstruction of: (a) (a' , a'') and (b) (c' , c''); cylindrical sample; Gaussian model function with $x_0 = 10$ mm, $y_0 = -10$ mm, and $r_0 = 30$ mm; 330 training and 100 testing points; $\bar{E} = 1.1\%$.

number of training points S_1 . It is seen that when S_1 is sufficiently large (in the present setting, nearly 250), the accuracy of the technique is about the same for both samples' configurations.

Operational capabilities of the technique are illustrated by the surfaces of actual Gaussian profiles of the dielectric constant and the respective reconstructed surfaces. In the examples in Fig. 10, the actual spatial distributions $\varepsilon'(x, y)$ in the rectangular sample are given by the following functions:

$$\varepsilon'(x, y) = 5 \left[1 + 0.5 \exp \left(-\frac{x^2 + y^2}{900} \right) \right] \quad (18)$$

$$\varepsilon'(x, y) = 5 \left[1 + 0.5 \exp \left(-\frac{x^2 + (y-30)^2}{900} \right) \right] \quad (19)$$

$$\varepsilon'(x, y) = 5 \left[1 + 0.5 \exp \left(-\frac{(x-30)^2 + (y-30)^2}{900} \right) \right]. \quad (20)$$

These surfaces are chosen to consider the profiles in which the maximum is located in the center of the domain, on its boundary, and in the corner. It is seen that the actual and reconstructed surfaces are very similar: the errors E/\bar{E} are equal to 0.087/1.4%, 0.033/0.6%, and 0.255/4.8% for surfaces (18)–(20), respectively.

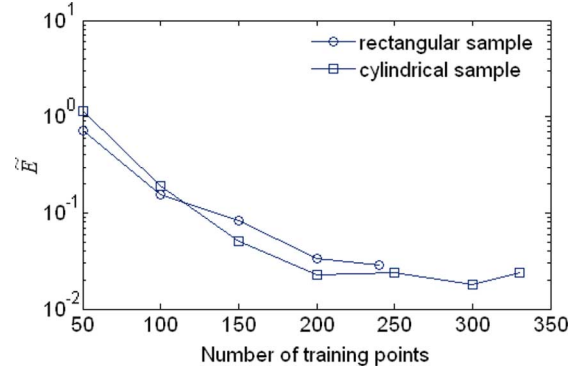


Fig. 9. Average total squared error (16) in the reconstruction of a' , a'' , d' , and d'' ; Gaussian model function with $x_0 = 10$ mm, $y_0 = -10$ mm, and $r_0 = 30$ mm.

TABLE I
AVERAGE ABSOLUTE AND AVERAGE RELATIVE ERRORS IN RECONSTRUCTION OF GAUSSIAN PROFILE OF DIELECTRIC CONSTANT (17) FROM TWO AND FOUR ROTATED POSITIONS OF THE RECTANGULAR SAMPLE

Number of training points	E/\bar{E} for $P=2$ (0 and 90°)	E/\bar{E} for $P=4$ (0, 90° , 180° , and 270°)
50	0.969/15.6%	0.781/12.6%
400	0.261/4.2%	0.233/3.8%

The results for the cylindrical sample are presented in Fig. 11—the actual surfaces described by the functions

$$\varepsilon'(x, y) = 5 \left[1 + 0.5 \exp \left(-\frac{(x+10)^2 + (y-10)^2}{900} \right) \right] \quad (21)$$

$$\varepsilon'(x, y) = 5 \left[1 - 0.5 \exp \left(-\frac{(x-20)^2 + y^2}{900} \right) \right] \quad (22)$$

are shown there along with the reconstructed ones; they are in very good agreement too: the level of closeness is characterized by E/\bar{E} equal to 0.112/1.4% (21) and 0.073/1.9% (22).

The overall accuracy achieved here in reconstruction of Gaussian profiles is notably higher than in the tests of [23]. This can be attributed to the more robust control over the model function's profiles provided by the independent parameters d' and d'' .

Accuracy of reconstruction is expected to be further improved for the samples with higher values of dielectric constant and with using more positions of the sample. The results of a computational experiment summarized in Table I show that when the tested sample in a waveguide is considered not at two, but at four positions rotated with respect to each other by 90° , reconstruction errors go down even if the number of training points is kept the same.

IV. DISCUSSION

The presented technique of waveguide microwave imaging is worth analyzing in a number of crucial aspects. In terms of network operations, the RBF ANN used for reconstruction of the permittivity profiles demonstrates excellent generalizing capabilities with the use of relatively small data sets in the databases of high dimensions. The examples given for the numbers of

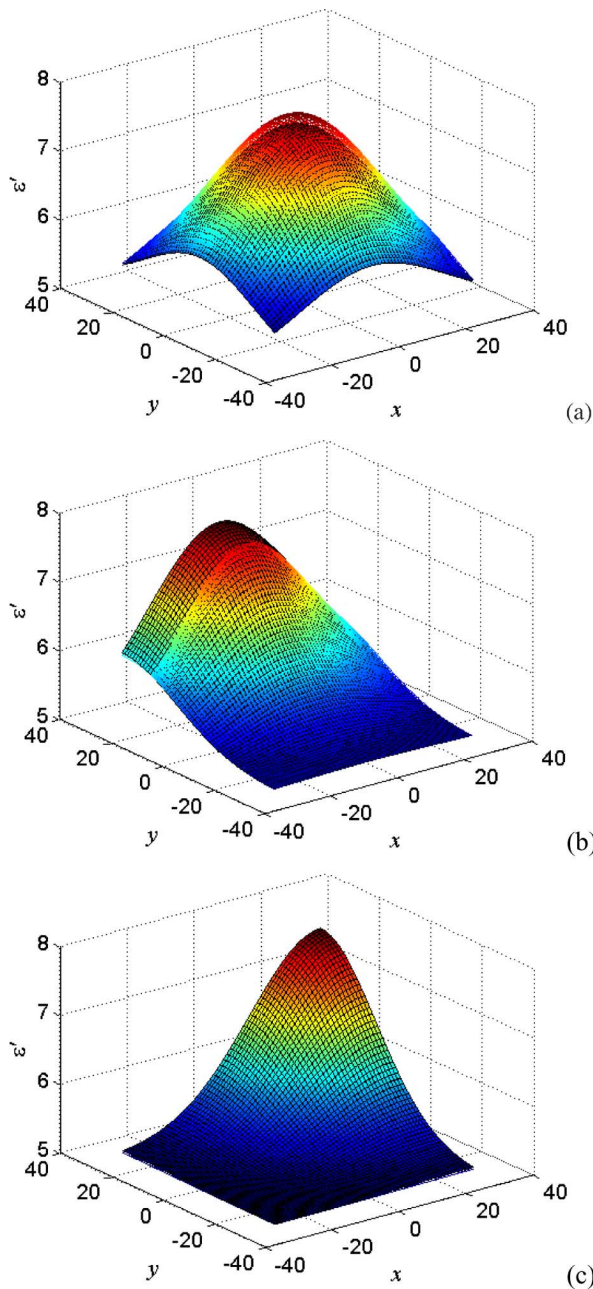


Fig. 10. Actual Gaussian profiles of dielectric constant (transparent surfaces) and reconstructed profiles (solid surfaces) for $\epsilon'(x, y)$ given by: (a) (18), (b) (19), and (c) (20); rectangular sample.

unknown six, six, and seven show a good accuracy of reconstruction of linear, quadratic, and Gaussian profiles from the databases of only 400, 476, and 330 points, respectively. Quality of profile reconstruction naturally depends on quality of network learning. The latter is easily controlled; in Section III, we present the examples in which the average errors achieved in reconstruction of linear, quadratic and Gaussian profiles in a rectangular sample ($\bar{E} = 0.4\%, 2.2\%$, and 4.8%) are obtained with the particular values of training error ($\hat{E} = 0.3\%, 2.6\%$, and 1.1%). Since the same type of RBF ANN has shown superior learning in determining complex permittivity of homogeneous samples [18], this network appears to be well suitable

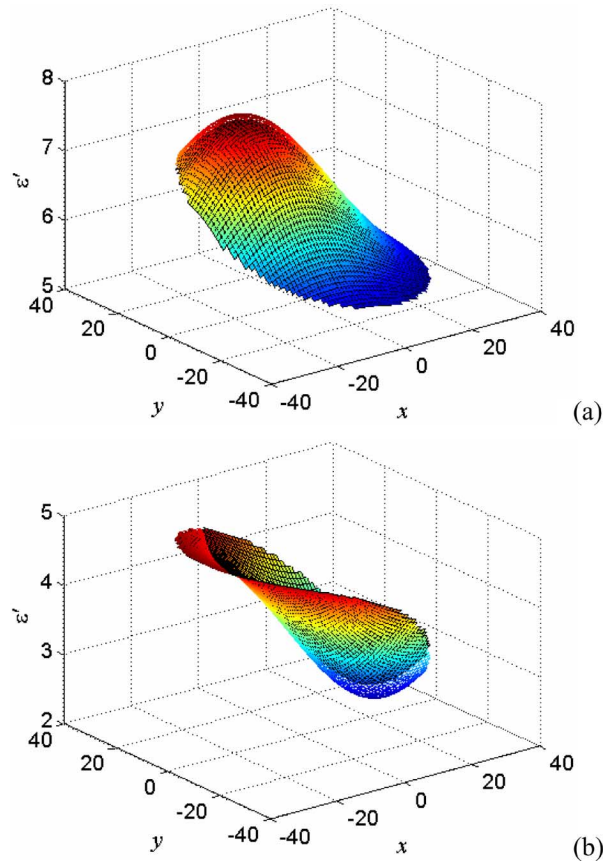


Fig. 11. Actual Gaussian profiles of dielectric constant (transparent surfaces) and reconstructed profiles (solid surface) for $\epsilon'(x, y)$ given by: (a) (21) and (b) (22); cylindrical sample.

for working in ANN-based techniques of waveguide microwave imaging.

It is worth emphasizing that in order to be operational as a general NDE technology and, in particular, be of practical use in applications involving microwave processing of materials, the proposed technique should be further developed to be able to reconstruct arbitrary 3-D permittivity profiles. Indeed, in the course of sintering of a powder compact, no prior knowledge of a function approximating spatial distributions of its material parameters may be available. A supposedly known functional approximation of the permittivity profile should, therefore, be considered as an assumption, which is introduced here as a necessary forced simplification on the way towards a “general technique” of waveguide microwave imaging. The idea of finding functional parameters instead of corresponding physical entities may be used in other ANN techniques of microwave imaging (including in open systems). On the other hand, the concept of approximation of the permittivity profile by a smooth function appears to be physically sensible being consistent with spatial distributions of material parameters of most sintered samples. For instance, experimentally and computationally obtained 2-D profiles of density and porosity of the samples of sintered ceramics [27], [28] are quite suitable for representation by smooth surfaces.

Another principal condition of functionality of this technique (as well as any other modeling-based method of determination

of material parameters, such as [17]–[19] and [29]–[31]) is the assumption that an analysis model generating numerical data adequately represents corresponding experimental setup in all its operational regimes. The one- and two-port versions of the method featuring similar ANN inversion and reconstructing complex permittivity of homogeneous samples have been reported in [18] and [19] in full experimental implementations. The techniques of [18], [19], and this paper are based on the same fundamental concept—the network is trained and tested with S -parameters obtained by 3-D FDTD modeling, and complex permittivity is determined from measured S -parameters. In [19], a number of practice-related issues (including sample orientation, low values of dielectric constant and the loss factor, etc.) have been resolved. This ensures good prospects for easy experimental implementation of the proposed technique in the WR975 measurement system [19].

More specifically, while it has been demonstrated that capabilities of the QuickWave-3D package allow for tuning corresponding FDTD models so as to accurately represent the measurements for all the desired scenarios [18], [19], the actual measured data can be noise contaminated and affect the accuracy of reconstruction. To handle this issue, the technique could be upgraded by switching to an inverse ANN proved to be efficient in reconstructing material parameters from imperfect (noisy) data on S -parameters [19].

Finally, it should be noted that the developed technique is based on the conjecture traditionally accepted in modeling-based techniques of determining material parameters in closed systems (see, e.g., [17]–[19] and [29]–[31]) assuming that a numerical inversion from the measured data is unique. In this paper, we assume that two sets of S_{11} and S_{21} (for original and 90°-rotated positions) can uniquely determine the unknown functional parameters of the considered profile functions. Strictly speaking, it is still an open question whether sets of S -parameters of a closed system (a transmission line or a resonator) uniquely determine permittivity profiles. It has been only shown that the transmission and reflection coefficients uniquely determine complex permittivity in a homogeneous sample in a parallel-plane waveguide [32]. However, it is expected that uniqueness can also be proven for reconstruction of profiles in general waveguides.

Related complications in practical use of the techniques based on the assumptions of uniqueness may be associated with several solutions numerically close to each other. There could be situations when training the network results in ambiguous indications regarding where in the complex permittivity plane the sought solution could be. It has been found that this issue can be normally overcome by repeated training with the use of a denser database [19]. In this study, we did not experience any complications of this sort; the reconstructions shown in Figs. 5, 7, 10, and 11 were the only options. However, if there were several close solutions, we could overcome the problem by taking more measurements for the sample in different positions.

V. CONCLUSION

In this paper, we have presented an applied technique for reconstruction of 2-D distribution of complex permittivity in

the material samples from elementary measurements in a waveguide system. Our method is based on the approximation of the permittivity profile by a continuous function defined by a small number of coefficients and neural network reconstruction of either those coefficients, or functional values of ϵ' and ϵ'' at some points inside the sample. Excellent performance of the technique handling linear and quadratic polynomials and a Gaussian function as the model functions of complex permittivity in rectangular and cylindrical samples has been demonstrated.

The suggested modeling-based approach appears to be feasible: while a computational cost may be relatively high (in the considered examples, it is up to 16 h), it requires a very few elementary measurements. The technique can be used in real-time reconstruction of profiles of ϵ' and ϵ'' assuming that the FDTD computation is performed during the preceding offline phase of the method's operation.

The reconstruction of nonuniform spatial distribution of ϵ' and ϵ'' from measurement of S -parameters of a waveguide system has been made possible with minimal "resources" used, e.g., with only two (original and rotated by 90°) positions of the tested sample and with seven coefficients of the Gaussian functions. The proposed concept of reconstruction of functional parameters, therefore, appears to be promising, as it has the potential to improve the accuracy and resolution by applying more sophisticated approximating functions, working with more sample's positions, and including extended sets of functional parameters in network operations. The technique can thus be directly extended to the general case of complex permittivity profile reconstruction in 3-D.

ACKNOWLEDGMENT

A portion of this work was done when author A. V. Brovko was hosted (September–December 2007) by the Institute of Processes in Life Sciences, University of Karlsruhe (TH), Karlsruhe, Germany, as a DAAD Fellow. The authors are grateful to M. Rother and H. P. Schuchmann for insightful comments and discussions.

REFERENCES

- [1] R. Zoughi, *Microwave Testing and Evaluation*. Amsterdam, The Netherlands: Kluwer, 2000.
- [2] X. Li, S. K. Davis, S. C. Hagness, D. W. van der Weide, and B. D. Van Veen, "Microwave imaging via space-time beamforming: Experimental investigation of tumor detection in multilayer breast phantoms," *IEEE Trans. Microw. Theory Tech.*, vol. 52, no. 8, pp. 1856–1865, Aug. 2004.
- [3] G. Bindu and K. T. Mathew, "Characterization of benign and malignant breast tissues using 2-D microwave tomographic imaging," *Microw. Opt. Technol. Lett.*, vol. 49, no. 10, pp. 2341–2345, 2004.
- [4] K. Belkebir, R. E. Kleinman, and C. Pichot, "Microwave imaging—Location and shape reconstruction from multifrequency scattering data," *IEEE Trans. Microw. Theory Tech.*, vol. 45, no. 4, pp. 469–476, Apr. 1997.
- [5] N. Qaddoumi, G. Carrière, S. Ganchev, and R. Zoughi, "Microwave imaging of thick composite panels with defects," *Mater. Eval.*, vol. 53, no. 8, pp. 926–929, 1995.
- [6] M. Pastorino, A. Salvade, R. Monleone, T. Bartesaghi, G. Bozza, and A. Randazzo, "Detection of defects in wood slabs by using a microwave imaging technique," in *IEEE Instrum. Meas. Tech. Conf.*, Warsaw, Poland, May 2007, pp. 1–6.
- [7] Y. V. Bykov, K. I. Rybakov, and V. E. Semenov, "High-temperature microwave processing of materials," *J. Phys. D, Appl. Phys.*, vol. 34, pp. R55–R75, 2001.

- [8] M. Gupta and E. W. W. Leong, *Microwaves and Metals*. Singapore: Wiley, 2007.
- [9] P. Mishra, G. Sethi, and A. Upadhyaya, "Modeling of microwave heating of particulate metals," *Metal. Mater. Trans. B*, vol. 37B, no. 5, pp. 839–845, Oct. 2006.
- [10] V. A. Mikhnev, E. Nufors, and P. Vainikainen, "Reconstruction of the permittivity profile using a nonlinear guided wave technique," *IEEE Trans. Microw. Theory Tech.*, vol. 45, no. 9, pp. 1405–1412, Sep. 1997.
- [11] O. A. M. Aly and A. S. Omar, "Reconstructing stratified permittivity profiles using super-resolution techniques," *IEEE Trans. Microw. Theory Tech.*, vol. 54, no. 1, pp. 492–499, Jan. 2006.
- [12] A. Ocera, E. Fratticcioli, M. Dionigi, and R. Sorrentino, "A novel technique for measuring one-dimensional permittivity profiles using a simple noncommensurate planar structure," *IEEE Microw. Wireless Compon. Lett.*, vol. 18, no. 3, pp. 155–157, Mar. 2008.
- [13] F. Akleman, "Reconstruction of complex permittivity of a longitudinally inhomogeneous material loaded in a rectangular waveguide," *IEEE Microw. Wireless Compon. Lett.*, vol. 18, no. 3, pp. 158–160, Mar. 2008.
- [14] S. Caorsi, G. L. Gragnani, and M. Pastorino, "Redundant electromagnetic data for microwave imaging of three-dimensional dielectric objects," *IEEE Trans. Antennas Propag.*, vol. 42, no. 5, pp. 581–589, May 1994.
- [15] M. Pastorino, "Short-range microwave inverse scattering techniques for image reconstruction and applications," *IEEE Trans. Instrum. Meas.*, vol. 47, no. 6, pp. 1419–1427, Dec. 1998.
- [16] S. Caorsi and M. Pastorino, "Two-dimensional microwave imaging approach based on a genetic algorithm," *IEEE Trans. Antennas Propag.*, vol. 48, no. 3, pp. 370–373, Mar. 2000.
- [17] R. Olmi, G. Pelosi, C. Riminesi, and M. Tedesco, "A neural network approach to real-time dielectric characterization of materials," *Microw. Opt. Technol. Lett.*, vol. 35, no. 6, pp. 463–465, 2002.
- [18] V. V. Yakovlev, E. K. Murphy, and E. E. Eves, "Neural networks for FDTD-backed permittivity reconstruction," *Int. J. Comput. Math. Elect. Electron. Eng.*, vol. 24, no. 1, pp. 291–304, 2005.
- [19] E. E. Eves, E. K. Murphy, and V. V. Yakovlev, "Practical aspects of complex permittivity reconstruction with neural-network-controlled FDTD modeling of a two-port fixture," *J. Microw. Power Electromagn. Energy*, vol. 41, no. 4, pp. 41.4-81–41.4-94, 2007.
- [20] F. Yaman and S. Simsek, "Neural network approach to determine non-smooth one-dimensional profiles in inverse scattering theory," *Microw. Opt. Technol. Lett.*, vol. 49, no. 12, pp. 3158–3162, 2007.
- [21] I. Elshafiey, L. Upda, and S. S. Upda, "Application of neural networks to inverse problems in electromagnetics," *IEEE Trans. Magn.*, vol. 31, no. 5, pp. 3629–3632, Sep. 1994.
- [22] A. V. Brovko, E. K. Murphy, M. Rother, H. P. Schuchmann, and V. V. Yakovlev, "Waveguide microwave imaging: Spherical inclusion in a dielectric sample," *IEEE Microw. Wireless Compon. Lett.*, vol. 18, no. 9, pp. 647–649, Sep. 2008.
- [23] A. V. Brovko, E. K. Murphy, and V. V. Yakovlev, "A neural network technique for reconstruction of 2D complex permittivity profiles of materials in waveguide systems," in *Proc. Global Congr. Microw. Energy Appl.*, Otsu, Japan, Aug. 2008, pp. 381–384.
- [24] E. K. Murphy and V. V. Yakovlev, "RBF network optimization of complex microwave systems represented by small FDTD modeling data sets," *IEEE Trans. Microw. Theory Tech.*, vol. 54, no. 7, pp. 3069–3083, Jul. 2006.
- [25] M. Kirby, *Geometric Data Analysis*. New York: Wiley, 2001.
- [26] QuickWave-3D QWED Sp. z o.o., Warsaw, Poland, 1988–2008. [Online]. Available: <http://www.qwed.com.pl>
- [27] T. Kraft, H. Riedel, and O. Rosenfelder, "Compaction and sintering of a ceramic seal: Modeling and experimental response," *Int. J. Powder Metall.*, vol. 39, no. 6, pp. 27–34, 2003.
- [28] A. Kuzmov, E. Olevsky, and A. Maximenko, "Multi-scale modelling of viscous sintering," *Model. Simul. Mater. Sci. Eng.*, vol. 16, 2008, Art. 035002 (10 pp).
- [29] R. Coccioli, G. Pelosi, and S. Selleri, "Characterization of dielectric materials with the finite-element method," *IEEE Trans. Microw. Theory Tech.*, vol. 47, no. 7, pp. 1106–1112, Jul. 1999.
- [30] K. P. Thakur and W. S. Holmes, "An inverse technique to evaluate permittivity of material in a cavity," *IEEE Trans. Microw. Theory Tech.*, vol. 49, no. 7, pp. 1129–1132, Jul. 2001.
- [31] J. Pitarch, M. Contelles-Cervera, F. L. Peñaranda-Foix, and J. M. Catalá-Civera, "Determination of the permittivity and permeability for waveguides partially loaded with isotropic samples," *Meas. Sci. Technol.*, vol. 17, pp. 145–152, 2006.
- [32] Y. V. Shestopalov and V. V. Yakovlev, "Uniqueness of complex permittivity reconstruction in a parallel-plane waveguide," *Radio Sci.*, vol. 42, 2007, Art. RS6S20 (6 pp).



Alexander V. Brovko (M'03) was born in Saratov, Russia, in 1972. He received the M.Sc. and Ph.D. degrees in radio physics and electronics from Saratov State University, Saratov, Russia, in 1996 and 1999, respectively.

From 1999 to 2005, he was an Assistant Professor and Associate Professor with Saratov State University. Since 2005, he has been with the Department of Applied Information Technologies, Saratov State Technical University, where he is currently Associate Professor. He has authored over 30 papers in referred

journals and conference proceedings. His research interests include computational electromagnetics, the finite-element method, the FDTD method, optimization techniques, microwave techniques, and optical devices.



Ethan K. Murphy received the B.S. degree in mathematics and M.S. degree in industrial mathematics from the Worcester Polytechnic Institute, Worcester, MA, in 2002 and 2003, respectively, and the Ph.D. degree in mathematics from Colorado State University, Fort Collins, in 2007.

He is currently a Research Assistant Professor with the Department of Mathematical Sciences, Worcester Polytechnic Institute. He has authored 20 papers in referred journals and conference proceedings. His research interests include inverse problems,

microwave optimization, microwave imaging, diffuse optical tomography, and electric impedance tomography.

Dr. Murphy is a member of the American Mathematical Society and Pi Mu Epsilon. He was a recipient of the 2002 WPI Provost Award for the Best Major Qualifying Project.



Vadim V. Yakovlev (M'05–SM'08) received the M.Sc. degree in radio physics and electronics from Saratov State University, Saratov, Russia, in 1979, and the Ph.D. degree in radio physics from the Institute of Radio Engineering and Electronics (IRE), Russian Academy of Sciences (RAS), Moscow, Russia, in 1991.

From 1984 to 1996, he was a Junior Research Scientist, Research Scientist, and Senior Research Scientist with IRE RAS. In 1993, he was a Visiting Researcher with the Centre "Les Renardières," Electricité de France. In 1996, he joined the Department of Mathematical Sciences, Worcester Polytechnic Institute (WPI), Worcester, MA, as a North Atlantic Treaty Organization (NATO)/National Science Foundation (NSF) Fellow. He has been with this Department since then, where he is currently a Research Associate Professor. He is a Head of the Industrial Microwave Modeling Group, which he established in 1999, as a division of the Center for Industrial Mathematics and Statistics, WPI. He has authored over 100 papers in referred journals and conference proceedings. His research interests in computational electromagnetics include neural network techniques for inverse problems, optimization, and microwave imaging, coupled electromagnetic/thermal problems, microwave power engineering, and broadband/multiband antennas. He has been a reviewer for several journals. In 2007, he was a Guest Editor of the "Special Issue on Modeling in Microwave Power Engineering" of the *Journal of Microwave Power and Electromagnetic Energy*. He is listed in the *1998 International Who's Who of Intellectuals* of the International Biographical Centre, Cambridge, U.K.

Dr. Yakovlev is a member of International Microwave Power Institute (IMPI). In 2004, he was inducted to the IMPI Technical Advisory Board. He is a member of the Association for Microwave Power in Europe for Research and Education (AMPERE) and a member of the Massachusetts Institute of Technology (MIT) Electromagnetics Academy. He is a member of program committees of several conferences.